

Frequency Domain Analysis for Extending Time Domain Reflectometry Water Content Measurement in Highly Saline Soils

Scott B. Jones* and Dani Or

ABSTRACT

Water content and electrical conductivity of soils are routinely determined using time-domain reflectometry (TDR) based on analysis of signal travel time and attenuation along embedded probes. In soils with appreciable salinity, time domain analysis becomes progressively inaccurate due to signal attenuation to the point of failure. Our objectives were to test whether dielectric permittivity, which is inextricable using TDR travel time analysis (TTA) in saline soils could be extracted using frequency domain techniques applied to waveforms from shorter TDR probes that reduce signal attenuation. The methodology was tested using coaxial cells and three-wire TDR probes in sand and silt loam soil under a wide range of saturated solution soil electrical conductivities. Three different interpretation techniques were compared; conventional TTA, scatter function fitting (SFF), and resonant frequency analysis (RFA). Using a range of probe lengths (2, 3, 6, 10, and 15 cm) soil bulk dielectric permittivity estimates were obtained using all three techniques in solution electrical conductivities up to 48 dS m^{-1} . Both SFF and RFA produced similar permittivity estimates, which generally increased with increasing solution electrical conductivity. Network analyzer permittivity measurements (0.5–1.5 GHz) were greater than estimates using TTA, which were both greater than values from SFF and RFA in a saturated silt loam soil. Although dependent upon dielectric permittivity and electrical conductivity, frequency domain analysis results indicate a 3-cm probe is optimal for maintaining an interpretable scatter function in the TDR frequency band while providing maximum extension of dielectric determination under lossy conditions in saturated soils.

TIME DOMAIN REFLECTOMETRY is gradually becoming one of the most accurate and reliable measurement methods for concurrent determination of bulk permittivity (ϵ_b) for water content and bulk electrical conductivity (σ_b) in soils and other porous media (Jones et al., 2002; Robinson et al., 2003b). However, even at moderate soil σ_b levels (typically at $\sigma_b \sim 2 \text{ dS m}^{-1}$) attenuation of the TDR signal degrades the ability to determine water content from TTA of the waveform (Fig. 1). The attenuation in soil is complex and proportional to σ_b , probe length, clay content and mineralogy, and water content. An alternative to travel time determination of the bulk dielectric permittivity (ϵ_b) is offered by transformation of the TDR waveform from the time to frequency domain, which is not based on waveform TTA. The key for implementation of such an approach is the potential use of very short TDR probes (e.g., $<10 \text{ cm}$, Jones and Or, 2001). Reduced probe length leads to increased measurement error using standard

TTA especially with the filtering of higher frequencies in cables longer than 3.2 m resulting in increased signal rise time (Heimovaara, 1993; Noborio, 2001). Timing or length measurement errors associated with finite pixel resolution can also be problematic. Shorter probes are appealing because losses due to electrical conductivity decrease proportionally with probe length reduction. Using TTA, Mojid (2002) compared water content determinations using three-rod TDR probes varying in length from 2 to 10 cm. Although waveforms deteriorated and became more trough-shaped and rounded with reduced probe length and water content, reasonable correlation to gravimetrically determined water content was found for all probes from 10 cm down to 2.5 cm in length. In contrast, Lin (2003b) showed a significant enhancement in the modeled bulk dielectric for probe lengths shorter than 10 cm in length while lengths between 10 and 50 cm showed little influence on permittivity. Persson and Haridy (2003) compared two-rod 2-cm long TDR probe measurements of σ_b and ϵ_b for estimating volumetric water content under constant soil solution electrical conductivity. Their third-order polynomial fit suggested improved accuracy using σ_b rather than dielectric measurements for water content determination with these short probes.

Time-domain methods employ a step voltage that propagates down a low-loss coaxial line, transitioning through fittings, multiplexers, and other lossy connections resulting in cumulative system losses acting as a low-pass filter that tends to spread the frequency content of the return signal seen by the TDR. The signal transition from the cable to the soil in the probe head is where the major mismatch in impedance occurs. The reflection from the end of the probe forms multiple reflections that result in a build-up of the waveform amplitude illustrated in Fig. 1. These undesirable losses in the system combine with electrical and dielectric losses we are interested in measuring in the soil. The total attenuation measured in the waveform at low frequencies (long distances) yields information on the soil's σ_b , but separation of the undesirable losses is difficult. Castiglione and Shouse (2003) recently demonstrated a difference reflection calibration method scaling σ_b measurements between an open and short-circuit of the TDR probe that removes unwanted system losses from the measurement of σ_b .

The extent to which electrical and even dielectric losses influence the measured bulk permittivity is not well understood and there seem to be three different views as to the effect of σ_b on ϵ .

Abbreviations: DFFT, discrete fast Fourier transform; EM, electromagnetic; NAM, network analyzer measurement; RFA, resonant frequency analysis; S_{11} , scatter function; SFF, scatter function fitting; TDR, time domain reflectometry; TTA, travel time analysis.

S.B. Jones, Dep. of Plants, Soils, and Biometeorology, Utah State Univ., Logan, UT 84322-4820; D. Or, Dep. of Civil and Environmental Engineering, Univ. of Connecticut, Storrs, CT 06269-2037. Received 29 Jan. 2004. *Corresponding author (scott.jones@usu.edu).

Published in Soil Sci. Soc. Am. J. 68:1568–1577 (2004).
© Soil Science Society of America
677 S. Segoe Rd., Madison, WI 53711 USA

1. Increased σ_b leads to reduced ϵ : Both conductive and imaginary losses identified by Topp et al. (2000) were suggested to reduce the real component of the water phase dielectric in soil. From a physical standpoint the reduction in the static permittivity in pure water in the presence of ions may arise from the hindered rotational nature of neighboring water molecules (Hasted et al., 1948).
2. Increased σ_b leads to constant ϵ : A number of studies have looked, at least in part, at the effects of σ_b on measured permittivity, revealing no significant influence on the measurement in soils (Topp et al., 1980; Dalton et al., 1984).
3. Increased σ_b leads to increased ϵ : Maxwell–Wagner effects that are more likely to occur at elevated σ_b and in high surface area porous media (i.e., where the ion migration path is relatively short) may enhance permittivity due to the dipole induced by accumulation of ions at interfacial surfaces (Hilhorst, 1998).

Harlow et al. (2003) found increased permittivity (due to faster travel time) for σ_b up to 5 dS m⁻¹ but saw no significant increase between 5 and 40 dS m⁻¹ using a time domain transmission technique. Lin (2003a) modeled increasing relative permittivity as a function of increasing σ_b in a parametric study using the Debye (1929) equation. Despite more than 20 yr of TDR measurement research in soils, conductive, and imaginary loss effects on dielectric measurements have not appeared significant in the relatively low σ_b range of measurement (<2 dS m⁻¹). Extending the σ_b range for measurements of permittivity by an order of magnitude or more using the technique proposed here or others will increase the possibility of an observable influence by ion concentration on the measured permittivity. It isn't certain what this effect will be given the complex interactions and competing phenomena described above.

Recent research has focused on the information content of the TDR waveform both in the time and frequency domains. A multi-section transmission line modeling approach for simulating TDR waveforms was shown to provide information on the soil's characteristic impedance (Feng et al., 1999). Other investigators have demonstrated how model parameters inferred in the frequency domain may provide information on frequency-dependent permittivity and electrical conductivity (Heimo-vaara et al., 1994; Friel and Or, 1999; Weerts et al., 2001; Lin 2003a, 2003b). Information on electrical conductivity, relaxation frequency, and dielectric permittivity parameterize models used to describe the frequency-dependent transformed waveform. The disadvantage of such an approach is the laborious process involving discrete fast Fourier transformation (DFFT) of the waveform and fitting of the appropriate model to the transformed scatter function. Fortunately this procedure can be automated to make it more amenable to real-time measurements.

The primary objective of this study was to determine the extent to which dielectric and electrical properties of saline soils and similar lossy porous media can be ex-

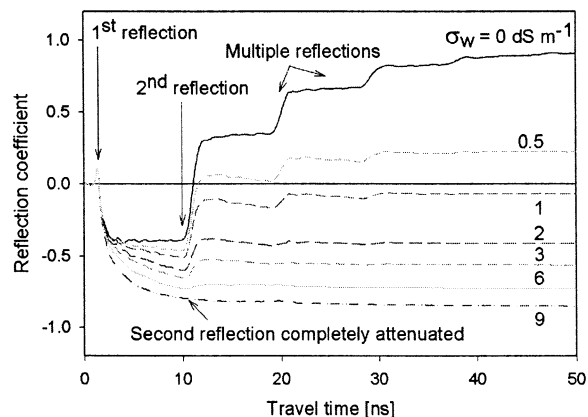


Fig. 1. Time domain reflectometry (TDR) waveforms measured in water using a coaxial TDR cell (20 cm) show progressive attenuation of the second reflection point with increasing solution electrical conductivity, σ_w , leading to eventual loss of permittivity (water content) determination.

tracted using TDR. We examined the following specific experimental methods: (i) transformation of the TDR waveform to the frequency domain via Fourier analysis, and (ii) using shorter TDR probes to reduce signal attenuation. Theoretically, we sought to improve time to frequency transformation by (i) comparing a ramping algorithm as a substitute for waveform differentiation and (ii) testing an alternative system input function for deriving the scatter function without the need for removable probe conductors (rods).

THEORY

Appropriate transformation of a TDR waveform from the time to the frequency domain yields the scatter function (S_{11}). The theoretical aspects of the transformation have been described in detail previously (Heimo-vaara et al., 1994; Friel and Or, 1999; Weerts et al., 2001; Huisman et al., 2002) and are only briefly reviewed here. As a TDR input signal, $v_0(t)$, traverses the waveguide (assumed coaxial), the response function, $r(t)$, represents interactions between the applied electromagnetic (EM) field and the sample. These interactions are summarized by the time-domain system response, $s(\tau)$, described by the following convolution integral (van Gemert, 1973)

$$r(t) = \int_{-\infty}^t v_0(t - \tau)s(\tau)d\tau \quad [1]$$

where τ is the variable of integration and $s(\tau)$ is dependent upon the cable, connectors, and coaxial sample holder and may be determined using fluids having a known response function. The DFFT reduces the convolution theorem integral to an algebraic written in terms of the frequency-dependent response, $R(f)$, system, $S_{11}(f)$, and input, $V_0(f)$, functions described by Lathi (1992) as

$$R(f) = V_0(f)S_{11}(f) \quad [2]$$

where f (Hz) is the frequency.

The measurement of reflections from a transmission line is a common method used in both time and frequency domain spectroscopy. In each case the signal is analyzed similarly with only the dependent variable differing (i.e., time or frequency). The multiple reflections of an open-ended coaxial transmission line can be modeled according to the scatter function given by Clarkson et al. (1977) as

$$S_{11}(f) = \frac{\rho + e^{-2\gamma L}}{1 + \rho e^{-2\gamma L}} \quad [3]$$

where ρ is the reflection coefficient described as

$$\rho = \frac{1 - z[\epsilon^*(f)]^{0.5}}{1 + z[\epsilon^*(f)]^{0.5}} \quad [4]$$

in which $z = z_c/z_p$ is the impedance ratio of the cable, z_c , and probe, z_p , and where γL is the transverse electromagnetic (TEM) mode propagation constant written as

$$\gamma L = \frac{i2\pi fL[\epsilon^*(f)]^{0.5}}{c} \quad [5]$$

in which L (m) is the probe length, c (m s^{-1}) is the speed of light and $\epsilon^*(f)$ may be described by the Debye (1929) model or a modified version by Cole and Cole (1941)

$$\epsilon^*(f) = \left[\epsilon_\infty + \frac{\epsilon_s - \epsilon_\infty}{1 + \left(i \frac{f}{f_{\text{rel}}}\right)^{(1-\beta)}} \right] - i \frac{\sigma_{\text{dc}}}{2\pi f \epsilon_0} \quad [6]$$

where ϵ_s is the static dielectric permittivity, ϵ_∞ is the permittivity at infinite frequency, f_{rel} is the dielectric relaxation frequency of the material, ϵ_0 is the permittivity of free space ($8.854 \times 10^{-12} \text{ F m}^{-1}$), σ_{dc} is the electrical conductivity and β ($0 \leq \beta \leq 1$) is a parameter added by Cole and Cole (1941) to describe the spread in relaxation frequency which tends to increase as the complexity of the mixture increases (e.g., minerals, biological materials). For pure liquids with a single relaxation frequency such as water or ethanol, β is zero resulting in the original Debye (1929) model.

MATERIALS AND METHODS

Experimental

A Tektronix 1502B cable tester (Tektronix Inc., Beaverton, OR) was used to obtain time domain reflectometry (TDR) waveforms. Waveforms were collected and analyzed using WINTDR99, an analysis software package (<http://soilphysics.usu.edu/wintdr>), which communicates with the TDR cable tester through an RS232 interface (Or et al., 2003). Time-domain reflectometry probes were used for measurements of solutions with a known dielectric constant (19-cm coaxial probe) and in a saturated sand and a saturated Millville silt loam soil (coarse-silty, carbonatic, mesic Typic Haploxerolls) (three-wire probes of length 2, 3, 6, 10, and 15 cm, see Fig. 2). Probe lengths were determined using the automated length calibration procedure in WINTDR99. Distilled water, ethanol, and octanol-1 were used as test solutions in a coaxial cell maintained at 25°C in a circulating water bath. Potassium chloride solutions of 0, 3, 6, 12, 18, and 24 dS m^{-1} were used to saturate the sand (bulk density, $\rho_b = 1.5 \text{ Mg m}^{-3}$) and in Millville silt loam soil ($\rho_b = 1.4 \text{ Mg m}^{-3}$) where concentrations of 36 and 48 dS m^{-1} were also used. A network analyzer (HP 8752C) with an HP 85070B dielectric probe attached was used to measure real and imaginary permittivity of KCl (3 dS m^{-1}) saturated Millville silt loam soil ($\rho_b = 1.4 \text{ Mg m}^{-3}$) for comparison between measured and modeled permittivities.

Analysis Procedure

The waveform transformation and analysis process is outlined in Fig. 3. It begins in the time domain with the input (v_o) and response (r) functions. The response function is the

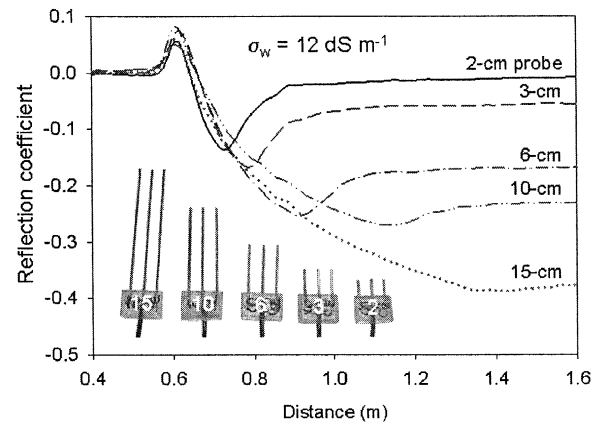


Fig. 2. Three-rod time domain reflectometry (TDR) probes ranging in size from 15 to 2 cm in length were used to obtain waveforms in Millville silt loam soil. Shorter probes are more effective in maintaining dielectric information based on the second reflection, which preserves critical scatter function features in the frequency domain.

waveform measured in soil that is typically measured using TTA under non-saline conditions. Using DFFT v_o and r are converted to the frequency domain where their ratio gives the scatter function (S_{11}). This transformation process along with the scatter function fitting (SFF) and resonant frequency analysis (RFA) are discussed in the following.

Waveform Acquisition

The waveform characteristics used for frequency domain analysis are a function of the sampling frequency and the total number of data points collected. Waveform transformation and processing requires accounting of distances or time associated with the discrete data from the time domain for proper transformation to the frequency domain. Each screen or window of the Tektronix 1502B or 1502C is divided into 10 divisions and contains a total of 251 points or pixels per window (pw). The process of collecting multiple waveforms may be automated using TDR control and analysis software and newer TDR devices may contain up to 2048 data points per window (Robinson et al., 2003b). The distance per division (dd) setting on the Tektronix 1502 adjusts the apparent window length, which for a distance per division setting of 0.25 m and 10 divisions per window (dw) is 2.5 m. Measurement frequency bandwidth, f_B , and sampling frequency, f_s , are two important considerations for establishing the measurement protocols in the time domain. The frequency bandwidth is computed from the rise time of the reflection, t_r , as $f_B = 0.35/t_r$ (Oliver and Cage, 1971). The sampling frequency of the measurement gives an indication of the measurement resolution, computed as

$$f_s = \frac{1}{\Delta t} = \frac{\text{pw} \times c \times V_p}{2\text{dd} \times \text{dw}} \quad [7]$$

where c is the speed of light in a vacuum, the 2 accounts for travel back and forth and V_p is the relative velocity of propagation (set to 0.99). The frequency bandwidth lies between f_s and the minimum frequency, f_{min} , calculated from the total waveform length in Table 1. Note that the computed value of f_s may exceed the actual operating bandwidth of the TDR cable tester, which for the 1502B is 2.5 GHz (Kelly et al., 1995). A sample calculation using eight waveforms sampled end to end with $\text{dd} = 0.25 \text{ m}$ yields 2008 total measured data points giving $f_{\text{min}} = 7.5 \text{ MHz}$ (i.e., $f_{\text{min}} = c/[2\text{dd} \times \text{dw} \times \text{nw}]$, where nw = number of windowed waveforms). The total num-

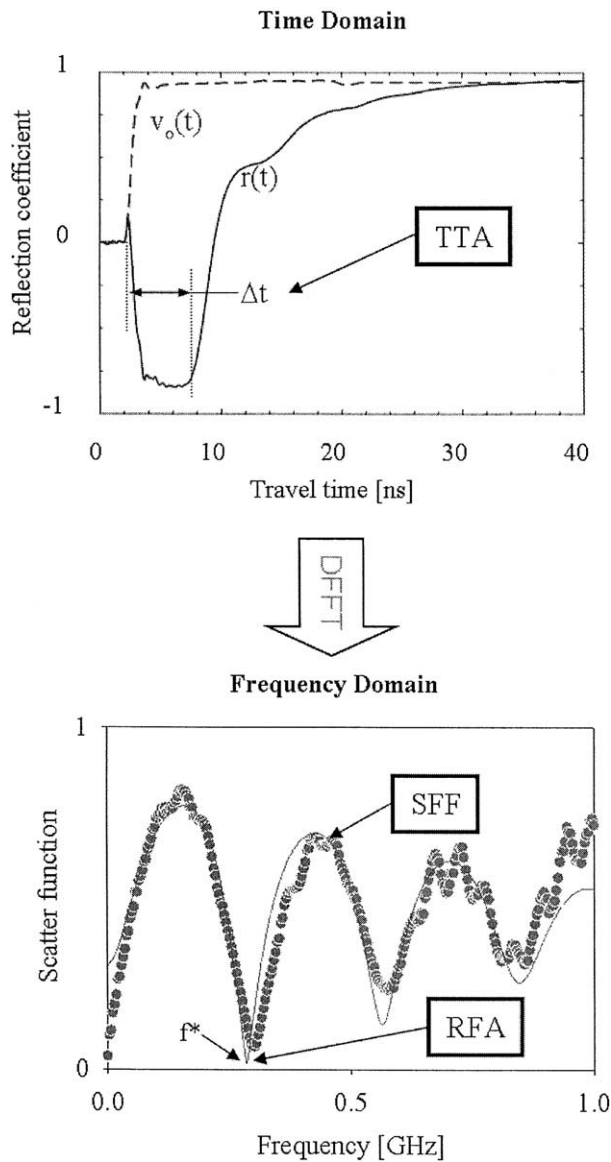


Fig. 3. Different modes of permittivity analysis are outlined in the waveform transformation process. Travel time analysis (TTA) yields permittivities in the time domain using longer probes in non-saline soils. Discrete fast Fourier transform (DFFT) of the input $[v_0(t)]$ and response $[r(t)]$ function waveforms provide the scatter function $[S_{11}(f)]$ from the transformed frequency-dependent functions $V_0(f)$ and $R(f)$. Permittivity estimates are obtained from scatter function fitting (SFF) utilizing Debye (1929) model parameterization or from resonant frequency analysis (RFA) giving permittivity estimates based on the resonant or half-wavelength frequency (f^*).

ber of data points in the final waveform, before Fourier transformation must be greater than or equal to the number of points in the original measured waveform, N , and equal to a positive integer power of 2 (i.e., 2^k where k is an integer). For the case of 2008 data points, the next largest value is 2048 (i.e., $2^{10} = 1024$ and $2^{11} = 2048$). The additional data points between 2048 and 2008 are assigned zeros or “zero-padded” in the time domain, which avoids aliasing errors and corresponds to ideal interpolation in the frequency domain. Aliasing errors occur when the sampling frequency of the waveform transformation is lower than twice the highest frequency contained in the signal (i.e., Nyquist frequency).

Table 1 summarizes the tradeoff between resolution (sampling frequency), which requires smaller dd settings, and frequency content (i.e., minimum frequency) requiring longer waveforms. Theoretically the instrument rise time (e.g., 150–300 ps) determines the maximum frequency contained in the TDR signal, in practice however, all porous media, cables and connectors act as low-pass filters, effectively removing higher frequencies and leading to a reduced reflected signal frequency content. The effective frequency bandwidth of the Tektronix 1502B was determined by Heimovaara et al. (1994) to lie in the range of 20 kHz to 1.5 GHz. For measurements in an attenuating soil, Friel and Or (1999) found a maximal frequency bandwidth of about 1 GHz.

The Input Function

Specification of the input function, $v_0(t)$, is required for the solution of the scatter function (Eq. [2]) in the frequency domain. The input function in the time domain describes the unaltered signal generated by the TDR and presumably propagating in the impedance matched cables along the transmission line to the beginning of the soil sample. It may be obtained by removing one of the conductors from the probe (Heimovaara et al., 1994) providing a distinct reflection at the probe-soil interface shown in Fig. 4. A more recent derivation of an input signal based on a waveform measured both with the central conductor removed, v_{oc} , and then shorted, v_{sc} , was suggested (Feldman et al., 1996) to be valid only for impedance-matched probes (Weerts et al., 2001), given as

$$v_0 = \frac{v_{oc} - v_{sc}}{2} \tag{8}$$

In either case, removal of one of the conductors is generally not practical using conventionally manufactured TDR probes. An alternate approach is to generate an artificial input function (v_a), which can be estimated using the waveform measured with the probe in air (Fig. 4). This provides an estimate of the initial rising slope of the input function waveform. This slope is important in determining the magnitude of the resulting scatter function, though it has less impact on the scatter function character (harmonics) important in characterizing permittivity. The slope is frequency dependent and largely influenced by cable length and may shift horizontal position as a result of cable temperature changes such as often occur in field applications (Robinson et al., 2003a). When represented in terms of the reflection coefficient, the distal point on the generated input function waveform is equal to 1. The artificially generated waveform, shown in Fig. 4, omits noise in the waveform caused by secondary reflections from the impedance change occurring in the head of the probe. A parametric expression for modeling $v_0(t)$ was suggested by Heimovaara (2001) and is labeled as the artificial input function, v_a . It is described using a time correction term, t_0 , designating the beginning of the rise in v_a and a term describing the inverse of the rise time of the pulse, α , given by

$$v_a = \frac{1 + erf[\alpha(t - t_0)]}{2} \tag{9}$$

The parameter α is estimated by fitting the rising slope of the artificial input function to that of a waveform measured in air.

Waveform Preparation and Discrete Fast Fourier Transformation

Time domain waveform transformation to the frequency domain is accomplished using a DFFT technique. The DFFT

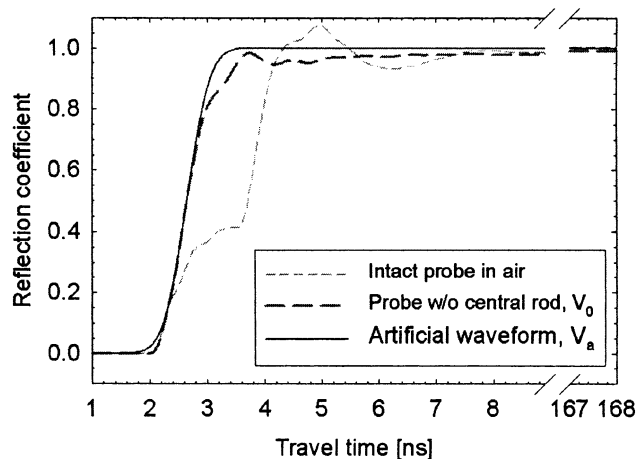


Fig. 4. Waveforms derived from TDR measurements using a three-wire probe in air and with no central conductor, v_0 , in addition to an artificially generated waveform, v_a . The input function can be represented by the waveform obtained with the central conductor removed or, as an alternative, it may be generated based on the initial rising slope of the waveform in air with a final value of 1.

is generally included as a standard function in modern mathematical software programs. Simply taking the DFFT of the waveform measured by the TDR is problematic because in a finite series the last point of the waveform is generally non-zero and introduces frequency errors. Heimovaara et al. (1994) used the backward differencing of the waveform with the assumption being that the derivative is zero at the beginning and end of the data. In general, noise is enhanced when the derivative of two similar quantities is taken in digital systems and therefore Nicolson (1973) suggested simply subtracting a ramp from the step response illustrated in Fig. 5. The linear ramp [i.e., $W(N) \times (n/N)$] is subtracted from the original waveform $W(n)$ at each point, n ($0 < n < N$), and is scaled according to the reflection coefficient of the final point in the waveform, N . To ensure a final value of zero the modified waveform, $W^*(n)$, is written $W^*(n) = W(n) - W(N) \times (n/N)$. A key feature of this algorithm is that the DFFT of $W^*(n)$ produces the same response as an infinite train of samples truncated out, so for frequencies $\omega = n\omega_0$, there is no error (Nicolson, 1973). After applying the Nicolson ramping algorithm or differentiating both input and response functions, waveforms are zero padded as described previously. The waveforms are transformed using DFFT yielding the frequency-dependent response function, $R(f)$, and input function, $V_0(f)$ that when divided yield the scatter function, $S_{11}(f)$, following Eq. [2].

Dielectric Permittivity Determination

The cyclical structure of the S_{11} harmonics provides definition needed for permittivity determination. One common approach is what we term scatter function fitting (SFF) using

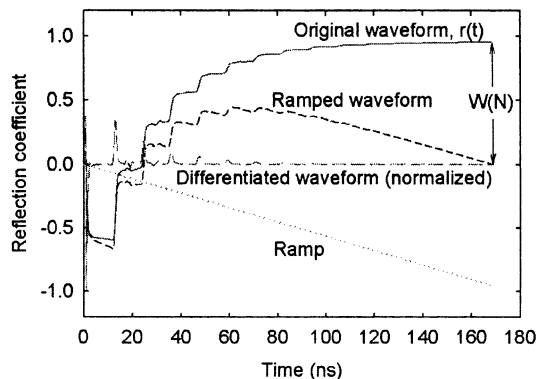


Fig. 5. Original response function waveform, $r(t)$, of water measured in a coaxial cell compared with the normalized differentiated waveform and the Nicolson ramped waveform. The ramped waveform results from taking the original waveform minus the ramp determined by the magnitude of $W(N)$, the distal point in $r(t)$ (Nicolson, 1973).

Eq. [5] through [8] from Clarkson et al. (1977). Since model parameters in Eq. [5] through [7] are known or measured, the complex permittivity is the only unknown and may be described using either Debye (1929) or Cole-Cole (Cole and Cole, 1941) models. Of the five coefficients parameterizing the Cole-Cole model (Eq. [6]), $\beta = 0$ gives the Debye model and σ_{DC} can be measured independently from signal attenuation in the time domain. The remaining parameters are ϵ_s , ϵ_∞ , and f_{rel} may serve as fitting parameters to fit Eq. [3] to the discrete S_{11} data. A detailed description and analysis for fitting Debye parameters to synthesized TDR waveforms was given by Weerts et al. (2001) and Lin (2003a). Details on parameter selection for inverse modeling of TDR waveforms are also described by Huisman et al. (2002). Due to the difficulty of locating a global minimum objective function in a multi-parameter optimization, only three parameters were allowed to vary where the objective function minimized the sum of squared differences between the transformed S_{11} measurements and the modeled S_{11} described by Eq. [3]. The constraints of the optimization were: $\beta = 0$, $\epsilon_\infty = 5$, $6 < \epsilon_s < 50$, $1e^7 \text{ Hz} < f_{rel} < 18e^9 \text{ Hz}$ and $0.01 \text{ dS m}^{-1} < \sigma_{DC} < 10 \text{ dS m}^{-1}$, with initial conditions $\epsilon_s = 30$, $f_{rel} = 2e^9 \text{ Hz}$ and $\sigma_{DC} = 0.1 \text{ dS m}^{-1}$. We used the static permittivity parameter to represent the measured bulk permittivity of a sample in our analysis assuming the relaxation frequency lies within or to the right of the TDR frequency bandwidth. This analysis is in contrast to the approach, by Weerts et al. (2001), who used ϵ_∞ to represent the bulk permittivity.

As an alternative to the multi-parameter fitting, we also evaluated a RFA approach based on S_{11} harmonics. Harmonics indicated by the real component of the S_{11} equal to -1 are related to the quarter-wavelength frequencies described by Heimovaara et al. (1996). We used the half-wavelength frequency indicated by 'troughs' in the magnitude of the complex scatter function to serve as markers for approximations of the

Table 1. Waveform minimum frequencies produced from different combinations of distance per division setting and waveform length expressed as points.

Distance per division	Sampling frequency	Time increment	Waveform length (points)			
			$2^9 = 512$	$2^{10} = 1024$	$2^{11} = 2048$	$2^{12} = 4096$
			Minimum frequency			
			MHz			
0.25	14.9	67	29.1	14.5	7.3	3.6
0.5	7.4	134	14.5	7.3	3.6	1.8
1	3.7	268	7.3	3.6	1.8	0.9

Table 2. Comparison of the normalized sum of squared errors (SSE) as a function of waveform preparation technique and input function for water and ethanol. The Debye modeled scatter function for water served as the reference S_{11} (25°C distilled water). Nicolson ramp and differentiation technique SSE values were almost identical comparing both input functions v_0 and v_a . The influence of rising slope error estimation in v_a on the resulting SSE is shown for both an increase and a decrease in slope of 25%.

Input function	Nicolson ramp water	Nicolson ramp ethanol	Differentiation water	Differentiation ethanol
v_0	1.00	1.00	1.00	1.00
v_a	1.11	0.92	1.10	0.92
$v_{a+25\%}$	1.19	0.82	1.18	0.82
$v_{a-25\%}$	1.17	1.13	1.17	1.13

dielectric permittivity, ϵ_x , which is inversely proportional to the square of the resonant frequency (f^*) and transmission path length for a reflection measurement, $2L$, given as

$$\epsilon_x = \left(\frac{nc}{2Lf^*} \right)^2 \quad n = 1 \dots \infty \quad [10]$$

Note that precise calibration of L and accurate determination of f^* is important when using shorter probes to reduce errors in ϵ estimation because the terms are squared in Eq. [10]. Both approaches for frequency domain analysis (i.e., SFF and RFA) are expected to provide dielectric information in lossy porous media where standard TDR-TTA fails.

RESULTS

Input Function Selection and Waveform Preparation

Waveforms were obtained from measurements in well-characterized liquids (i.e., water and ethanol) to compare different input function options and waveform preparation techniques. The use of an artificial input function, v_a , was compared with an input function measured in air using a coaxial or three-wire probe with no central conductor, v_0 , (see Fig. 4) and using water to generate the response function, r . The resultant scatter functions in each case (i.e., $R/V_a = S_{11,a}$ and $R/V_0 = S_{11,0}$) were compared with the modeled scatter function, $S_{11,cc}$, using known Cole–Cole parameters for water and ethanol (Friel and Or, 1999) as reference. The sum of squared errors (SSE) were obtained from the sum of differences squared (i.e., $[S_{11,cc} - S_{11,0}]^2$ and $[S_{11,cc} - S_{11,a}]^2$), over the frequency range from 3.6 MHz up to 1.2 GHz. The results shown in Table 2 demonstrate there is little difference between either of the two waveform preparation techniques (i.e., Nicolson ramp vs. Differentiation) and that the artificially generated input, v_a , is a reasonable alternative to the input function, v_0 , obtained with the central conductor removed.

We suggested earlier using the waveform of an intact probe measured in air to model the rising slope of v_0 (Fig. 4) using Eq. [9]. As a reference, we use the slope of v_0 , measured without the center conductor, and match the slope of v_a to v_0 . To test the influence of slope estimation errors on the SSE, we additionally imposed a slope error of $\pm 25\%$ in v_a and produced scatter functions using v_a , $v_{a+25\%}$, and $v_{a-25\%}$ thereafter computing the SSE comparing the Debye modeled S_{11} for water and ethanol.

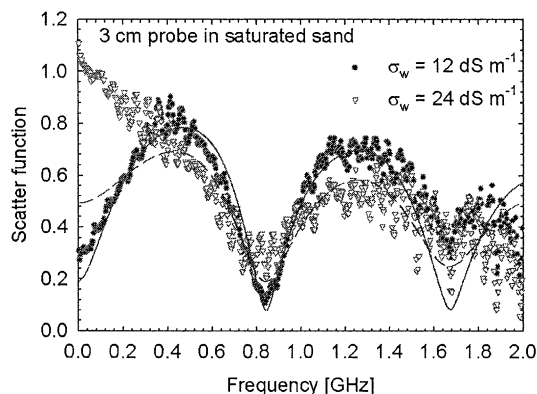


Fig. 6. Scatter functions derived from discrete fast Fourier transform (DFFT) of measured waveforms obtained using a three-wire time domain reflectometry (TDR) probe (3-cm) in saturated sand with $\sigma_w = 12$ and 24 dS m^{-1} . Lines represent Clarkston (1977)–Debye (1929) modeled scatter functions fit (SFF) to S_{11} data obtained in the time domain. Static permittivities (ϵ_s) determined for 12 and 24 dS m^{-1} were 28 and 29, respectively compared with a TTA measured dielectric of 29 under non-saline conditions.

Results presented in Table 2 show that the use of v_a as the input function provides both larger and smaller SSE values relative to v_0 . Errors in slope estimation of $\pm 25\%$ appear to double the error associated with v_a as input for the scenarios tested here. Our analysis showed that the amplitude and slope of the S_{11} to be the major effect introduced by perturbations in the slope of the artificial input function. The error introduced using an artificial input function on permittivity estimation appears to be minor because the permittivity determination is largely a function of the scatter function wavelength.

Scatter Function Fitting

Three-wire TDR probes were used to obtain waveforms in saturated sand with different solution electrical conductivities. The resulting scatter functions using a 3-cm probe with two different σ_w levels are illustrated in Fig. 6 where the S_{11} harmonic signature and amplitude diminish with increasing σ_w . Despite the increased dispersion of the data beyond about 1.5 GHz (practical upper frequency range), there is sufficient definition (i.e., amplitude) in the scatter function for reliable fitting of the Cole–Cole or Debye models. The dominant fitting features in the S_{11} for extracting permittivity information are the ‘trough’ locations referred to as half-wavelength frequencies, which are related to probe length and permittivity. For an increase in probe length and in solution electrical conductivity, σ_w , signal attenuation becomes greater and the effect is reduced S_{11} amplitude and integrity, and eventually fitting fails due to both a lack of definition in the S_{11} data and in the modeled S_{11} . The S_{11} character is preserved to much higher σ_w levels in the frequency domain than the waveform second reflection in the time domain under similar conditions.

Resonant Frequency Analysis

Resonant frequency analysis relies on the half-wavelength frequency described in Eq. [10]. Figure 7 shows S_{11} data for 12 and 48 dS m^{-1} solution electrical conduc-

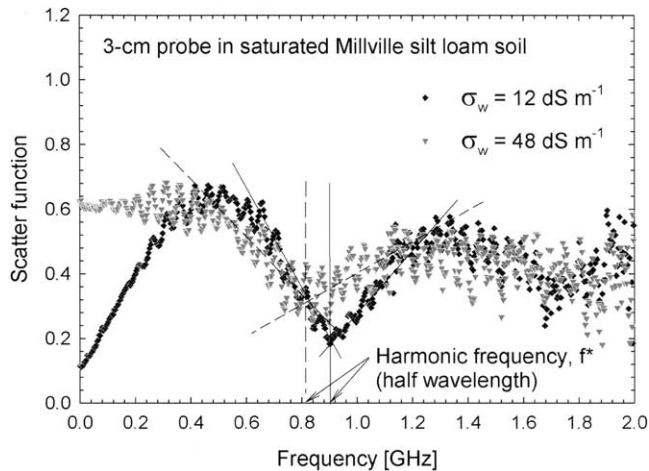


Fig. 7. Scatter function obtained in saturated Millville silt loam at two different salinity levels using a 3-cm long three-wire probe. Resonant frequency analysis (RFA) of the 48 dS m⁻¹ scatter function using the intersection of two lines drawn through the rising portion of the scatter function data in the first trough yields a permittivity, ϵ_s , of 30.2 following Eq. [10]. This is comparable with the static permittivity ($\epsilon_s = 29.9$) obtained from fitting the Debye (1929) model to this data.

tivity in Millville silt loam using a 3-cm probe. To illustrate RFA, we analyze the 48 dS m⁻¹ scatter function in Fig. 7 where the harmonic trough in the S_{11} corresponds to an approximate frequency of 0.84 GHz. The resulting permittivity using $L = 0.03$ m and $f^* = 0.84$ GHz is 35.4 using Eq. [10]. Using a more precise determination of L (0.0335 m) and $f^* = 0.815$ GHz, obtained by fitting tangent lines through the rising scatter function data on both sides of the estimated f^* value, yields a value of $\epsilon_s = 30.2$, which is much closer to the Debye modeled value ϵ_s of 29.9. Calibration of the probe length, L , was suggested to be more accurate using measurements in air and water at known temperature (Robinson et al., 2003b). The determination of ϵ using the RFA approach provides a more rapid though less informative method for permittivity evaluation, forgoing the fitting procedure using parameters of the Cole–Cole or Debye models.

A summary of the bulk permittivity determinations using SSF and TTA are compared in Fig. 8 for both saturated Millville silt loam and sand where each determination is given as a function of solution electrical conductivity. As a reference, we refer to the TTA determinations obtained using the 15-cm probe ($\sigma_w = 0$ dS m⁻¹), which were approximately 27 and 29, respectively. In the frequency domain analysis using SFF shown in Fig. 8a and 8c, permittivity determinations using longer probes fail and diverge as a function of probe length. All determinations using SFF are below the reference values using TTA at lower σ_w . Individual scatter functions for the 3-cm probe contained the greatest detail for analysis of permittivity extending determinations to higher σ_w levels approaching 50 dS m⁻¹. Results from the 2-cm probe gave slightly lower permittivity estimates, which likely resulted from the half-wavelength extending beyond the TDR frequency range (e.g., >1 GHz). Topp et al. (2000) attributed the increased per-

mittivity from TDR measurements in soils to the presence of ions in solution (dc conductivity) and to dielectric losses. The benefit of extending the permittivity measurement range under saline conditions comes at the sacrifice of time domain analysis capability, where shorter probes suffer from reduced accuracy or fail completely using TTA evidenced by the lack of data in Fig. 8b and 8d. All TTA results diverge for solution electrical conductivities greater than 12 dS m⁻¹ and also show a general increase in ϵ_b with increasing σ_b .

In Fig. 9, results from RFA analysis are compared with SFF with a 1:1 line plotted as reference. Filled symbols represent measurement in Millville silt loam, which are generally over predicted using RFA compared with SFF. Determinations in sand (empty symbols) show improved correlation between the two frequency domain methods.

Comparison of TDR and Network Analyzer Measured Permittivities

Permittivities determined using TTA of TDR waveforms result from a lumped frequency band that is a function of many factors (e.g., bound and free water content, media characteristics, cable tester characteristics) and lies within the range of 20 kHz to 1.5 GHz for the Tektronix cable tester (Heimovaara et al., 1994). Permittivity values obtained from time domain analysis and frequency domain analysis of the waveforms using a 19.6-cm coaxial cell were compared with network analyzer measurements (NAM). Real NAM permittivities at 0.5, 1.0, and 1.5 GHz frequencies are listed in Table 3 for saturated Millville silt loam soil at temperatures of 5, 25, and 45°C. Network analyzer measurements values decrease with increasing temperature as expected from the dielectric temperature response of free water. The higher measurement accuracy associated with TDR using TTA shows reduced ϵ_b but with a similar temperature-dependent response to the NAM values. Dielectric determinations using SFF and RFA produced a temperature response that was opposite or inconsistent with expectations, but overall, reasonable correlation was found with all four measurement techniques.

Additional Considerations and Limitations

The use of short TDR probes coupled with frequency domain analysis of TDR waveforms facilitates an extension of permittivity measurements at higher levels of soil bulk electrical conductivity (salinity). In spite of complications in processing waveforms and fitting model parameters, which requires a number of steps including Fourier analysis and optimization, much of the procedure may be automated for rapid processing and direct output using TDR analysis software. The inference of water content from permittivity determination using short probes and frequency domain analysis will likely require more effort than application of the commonly used equation of Topp et al. (1980). In addition to the influence of bound water common in clayey soils, ionic conduction, and potentially Maxwell–Wagner effects will be greatly magnified and may artificially enhance

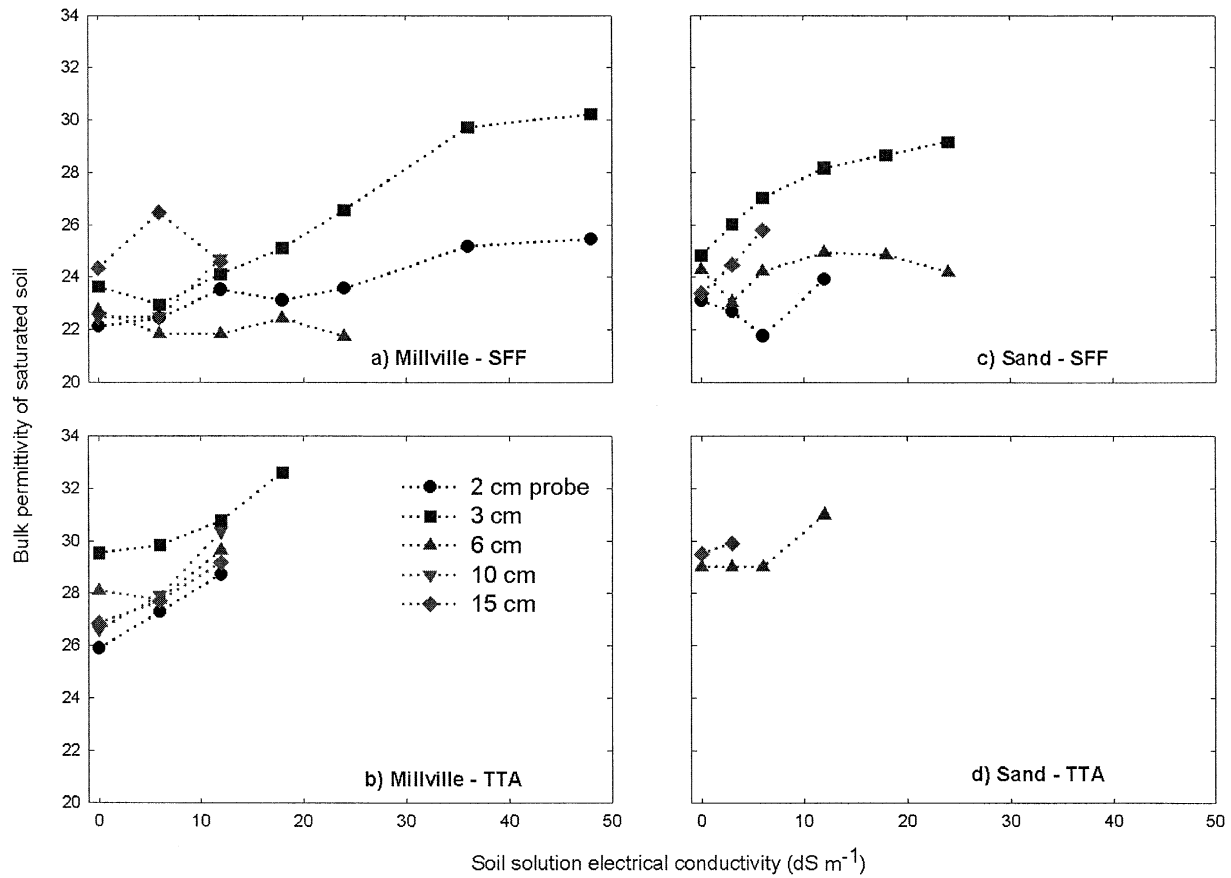


Fig. 8. Bulk permittivity of Millville silt loam and sand determined using scatter function fitting (SFF) in the frequency domain and travel time analysis (TTA) in the time domain given as a function of soil solution electrical conductivity. To illustrate the effect of signal attenuation on permittivity determination, probe lengths of 2, 3, 6, 10, and 15 cm were used (note: 10-cm probe was not used in sand).

or otherwise alter the measurement of permittivity. Advanced and perhaps more comprehensive modeling approaches are needed for a rigorous and physically based permittivity-water content relationship in high surface area and lossy porous media.

Physical limitations of the frequency domain analysis approach are demonstrated in Fig. 10 using a plot of the relationship between probe length, resonant frequency and permittivity from Eq. [10]. The interplay between probe length and resonant frequency suggests that as permittivity decreases (drier soil) the minimum probe length (resonant frequency) increases, which narrows the useful range of frequency domain analysis under lower permittivity or dryer conditions. This limitation, however, is offset by the commensurate reduction in bulk soil electrical conductivity that occurs with decreasing soil water content. Optimal probe length is largely a function of measurement frequency, signal attenuation and porous medium dielectric with 10- to 15-cm probes lengths being optimal for non-saline soils and probes as short as 3-cm for saline soils or lossy conditions. This ‘optimal’ probe length is bounded by

frequency and permittivity from Eq. [10]. The interplay between probe length and resonant frequency suggests that as permittivity decreases (drier soil) the minimum probe length (resonant frequency) increases, which narrows the useful range of frequency domain analysis under lower permittivity or dryer conditions. This limitation, however, is offset by the commensurate reduction in bulk soil electrical conductivity that occurs with decreasing soil water content. Optimal probe length is largely a function of measurement frequency, signal attenuation and porous medium dielectric with 10- to 15-cm probes lengths being optimal for non-saline soils and probes as short as 3-cm for saline soils or lossy conditions. This ‘optimal’ probe length is bounded by

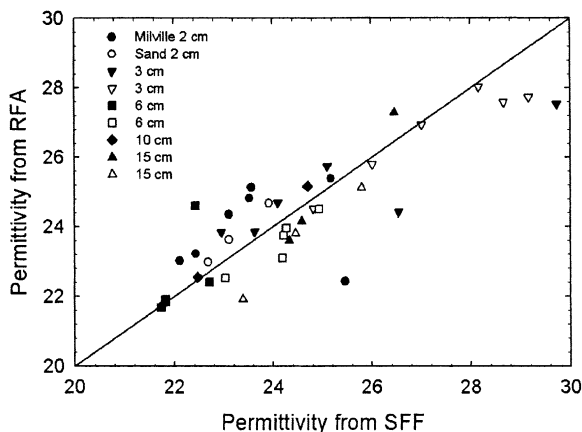


Fig. 9. One to one comparison between scatter function fitting (SFF) and resonant frequency analysis (RFA) techniques for permittivity determination in the frequency domain. Filled symbols represent determinations in Millville silt loam and empty symbols are for sand.

Table 3. Temperature-dependent permittivities determined by travel-time analysis (TTA, ϵ_s), scatter function fitting (SFF, ϵ_s), resonant frequency analysis (RFA, ϵ_x), and network analyzer measurements (NAM, ϵ') of the real permittivity measured at 0.5, 1.0, and 1.5 GHz. Time domain reflectometry measurements were made in 19.6-cm coaxial cells packed with Millville silt loam saturated with a KCl solution electrical conductivity of 3 dS m⁻¹.

Temperature °C	TTA		RFA	NAM		
	ϵ_b	ϵ_s	ϵ_x	ϵ' at 0.5 GHz	ϵ' at 1 GHz	ϵ' at 1.5 GHz
5	27.4	26.4	25.8	29.7	29.3	29.0
25	26.6	25.5	24.9	28.6	28.2	27.9
45	25.2	25.8	26.5	27.0	26.4	26.0

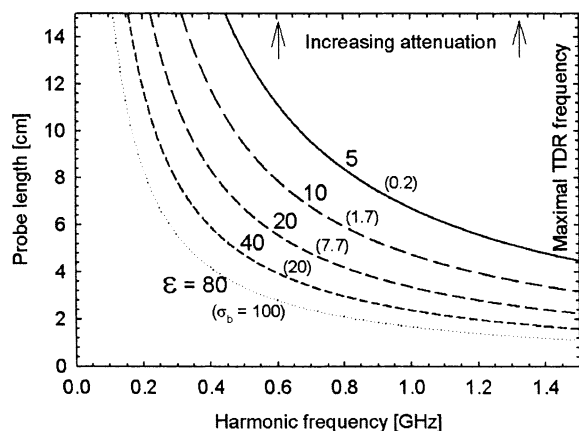


Fig. 10. Contour lines of resonant frequency-probe length are given as a function of permittivity and suggest bounds for using short probes (i.e., also bounded by maximal TDR frequency and by increasing attenuation). Numbers in parentheses are computed soil electrical conductivities estimated using Eq. [11] ($\sigma_w = 110 \text{ dS}^{-1}$) and the permittivity-water content relation (Eq. [12]) given by Topp et al. (1980). Reduced permittivity (water content) leads to a commensurate reduction in σ_b , suggesting that there may be regions of overlap where TTA and SFF using short probes are applicable.

greater attenuation with increasing probe length and maximum signal frequency (e.g., below 1.5 GHz for TDR).

The magnitude of the change in electrical conductivity as a function of water content inferred from permittivity can be illustrated using a simplifying example. We apply the empirical relationship of Topp et al. (1980) describing the volumetric water content (θ_v) of mineral soils in terms of ϵ_b , written as

$$\theta = -5.3 \times 10^{-2} + 2.92 \times 10^{-2} \epsilon_b - 5.5 \times 10^{-4} \epsilon_b^2 + 4.3 \times 10^{-6} \epsilon_b^3 \quad [11]$$

This equation may be combined with a relationship describing σ_b written in terms of σ_w , the soil volumetric water content (θ_v), and saturated water content (θ_{sat}), given as (Mualem and Friedman, 1991)

$$\sigma_b = \sigma_w \left(\frac{\theta_v}{\theta_{\text{sat}}} \right)^{2.5} \quad [12]$$

The bulk electrical conductivity was computed for a hypothetical medium with a porosity of 1 and an electrical conductivity of the solution of 110 dS m^{-1} for illustration purposes (i.e., yielding $\sigma_b = 100$ for $\theta_v = 0.96$ given $\epsilon_b = 80$ from Eq. [11]). Computed σ_b values are shown in parentheses in Fig. 10 and correspond to permittivity values shown. These estimates demonstrate the three-order magnitude reduction in σ_b with a linear decrease in ϵ_b values of from 80 to 5. The non-linear reduction in σ_b suggests that under certain conditions both frequency domain and TTAs may be simultaneously compatible (e.g., under moderate σ_b levels).

CONCLUSIONS

Time- to frequency-domain transformation of TDR waveforms coupled with frequency domain analysis extends the range of bulk permittivity measurement in

saline soils. Use of an artificially generated step function in the time domain provides a convenient and rapid means of generating the required input signal $[v(t)]$ while avoiding the need for a removable conductor. The Nicolson ramping algorithm provides a robust alternative method for preparing waveforms for discrete fast Fourier transform and produces results similar to those obtained using waveform differentiation. Information on sample dielectric permittivity is preserved in the frequency domain for lossy media with electrical conductivities approaching levels five times greater than the upper limit in the time domain. This enhancement of recoverable information is attainable using short TDR probes (to reduce signal attenuation) and time- to frequency-domain transformation of the waveform. A comparison of SFF and RFA techniques exhibited similar permittivity determinations by each in both sand and silt loam soil. Precise calibration of probe length (especially using shorter probes as compared with long probes in the time domain) and resonant frequency are critical when using the simplified calculation in Eq. [10]. Optimal measurements are largely a function of probe length, signal attenuation and porous medium dielectric with 10- to 15-cm probe lengths being optimal for conventional measurements in the time domain and probes as short as 3 cm for highly lossy conditions when considering frequency domain analysis. Critical scatter function characteristics using a 2-cm probe were partially lost as the resonant frequency approaches the upper TDR frequency band. The procedure outlined here can be automated and implemented as a subroutine in TDR measurement and analysis software. Refinement of probe characteristics (length, geometry) for reducing S_{11} noise and automation and refinement of fitting procedures are areas of ongoing research.

ACKNOWLEDGMENTS

The authors gratefully acknowledge research grants from the Israel-US Binational Agricultural Research and Development (BARD) Fund (Project IS-2839-97) and from Campbell Scientific and HarvestMaster (Logan, UT). This material is based in part upon work supported by the Cooperative State Research, Education, and Extension Service, U.S. Department of Agriculture, under Agreement No. 2002-35107-12507. We express appreciation to Seth Humphries and Bill Mace for their assistance with data analysis and experiment preparation.

REFERENCES

- Castiglione, P., and P.J. Shouse. 2003. The effect of ohmic cable losses on time-domain reflectometry measurements of electrical conductivity. *Soil Sci. Soc. Am. J.* 67:414-424.
- Clarkson, T.S., L. Glasser, R.W. Tuxworth, and G. Williams. 1977. An appreciation of experimental factors in time-domain spectroscopy. *Adv. Mol. Relax. Interact. Processes* 10:173-202.
- Cole, K.S., and R.H. Cole. 1941. Dispersion and adsorption in dielectrics: I—Alternating current characteristics. *J. Chem. Phys.* 9:341-351.
- Dalton, F.N., W.N. Herkelrath, D.S. Rawlins, and J.D. Rhoades. 1984. Time-domain reflectometry: Simultaneous measurement of soil water content and electrical conductivity with a single probe. *Science* 224:989-990.
- Debye, P. 1929. *Polar molecules*. Dover, Mineola, New York.
- Feldman, Y., A. Andrianov, E. Polygalov, I. Ermolina, G. Romanychev, Y. Zuev, and B. Milgotin. 1996. Time domain dielectric spec-

- troscopy: An advanced measuring system. *Rev. Sci. Instrum.* 67: 3208–3216.
- Feng, W., C.P. Lin, R.J. Deshamps, and V.P. Drnevich. 1999. Theoretical model of a multisection time domain reflectometry measurement system. *Water Resour. Res.* 35:2321–2331.
- Friel, R., and D. Or. 1999. Frequency analysis of time-domain reflectometry (TDR) with application to dielectric spectroscopy of soil constituents. *Geophysics* 64:1–12.
- Harlow, R.C., E.J. Burke, and T.P.A. Ferre. 2003. Measuring water content in saline sands using impulse time domain transmission techniques. *Vadose Zone J.* 2:433–439.
- Hasted, J.B., D.M. Ritson, and C.H. Collie. 1948. Dielectric properties of aqueous ionic solutions: Part I. *J. Chem. Phys.* 16:1–11.
- Heimovaara, T.J. 2001. Frequency domain modeling of TDR waveforms in order to obtain frequency-dependent dielectric properties of soil samples: A theoretical approach. In C.H. Dowding (ed.) *Proc. of the Second International Symposium and Workshop on Time Domain Reflectometry for Innovative Geotechnical Applications*. Available at <http://www.iti.northwestern.edu/tdr/tdr2001/proceedings/Final/TDR2001.pdf> (verified 24 May 2004). Infrastructure Technology Institute, Northwestern University, Evanston, IL.
- Heimovaara, T.J. 1993. Design of triple-wire time domain reflectometry probes in practice and theory. *Soil Sci. Soc. Am. J.* 57:1410–1417.
- Heimovaara, T.J., W. Bouten, and J.M. Verstraten. 1994. Frequency domain analysis of time domain reflectometry waveforms: 2. A four-component complex dielectric mixing model for soil. *Water Resour. Res.* 30:201–209.
- Heimovaara, T.J., E.J.G.D. Winter, W.K.P. van Loon, and D.C. Esveld. 1996. Frequency-dependent dielectric permittivity from 0 to 1 GHz: Time domain reflectometry measurements compared with frequency domain network analyzer measurements. *Water Resour. Res.* 32:3603–3610.
- Hilhorst, M.A. 1998. Dielectric characterization of soil. Ph.D. Diss. Wageningen Agricultural University, Wageningen, the Netherlands.
- Huisman, J.A., A.H. Weerts, T.J. Heimovaara, and W. Bouten. 2002. Comparison of travel time analysis and inverse modeling for soil water content determination with time domain reflectometry. *Water Resour. Res.* 38(6), 1077, doi:10.1029/2001WR000259, 2002.
- Jones, S.B., and D. Or. 2001. Extending TDR measurement range in saline soils using frequency domain methods. p. 140–148. In C.H. Dowding (ed.) *Proc. of the Second International Symposium and Workshop on Time Domain Reflectometry for Innovative Geotechnical Applications*, available at <http://www.iti.northwestern.edu/tdr/tdr2001/proceedings/Final/TDR2001.pdf>. (verified 24 May 2004.) Infrastructure Technology Institute, Northwestern University, Evanston, Illinois.
- Jones, S.B., J.M. Wraith, and D. Or. 2002. Time domain reflectometry (TDR) measurement principles and applications. *Hydrol. Processes* 16:141–153.
- Kelly, S.F., J.S. Selker, and J.L. Green. 1995. Using short soil moisture probes with high-bandwidth time domain reflectometry instruments. *Soil Sci. Soc. Am. J.* 59:97–102.
- Lathi, B.P. 1992. *Linear signal and system analysis*. Cambridge Press, Berkeley.
- Lin, C.P. 2003a. Frequency domain versus travel time analyses of TDR waveforms for soil moisture measurements. *Soil Sci. Soc. Am. J.* 67:720–729.
- Lin, C.P. 2003b. Analysis of nonuniform and dispersive time domain reflectometry measurement systems with application to the dielectric spectroscopy of soils. *Water Resour. Res.* 39:1012.
- Mojid, M.A. 2002. Practical considerations on the use of down-sized time-domain reflectometry (TDR) probes. *Hydrol. Earth Syst. Sci.* 6:949–955.
- Mualem, Y., and S.P. Friedman. 1991. Theoretical prediction of electrical conductivity in saturated and unsaturated soil. *Water Resour. Res.* 27:2771–2777.
- Nicolson, A.M. 1973. Forming the fast Fourier transform of a step response in time-domain metrology. *Electronics Lett.* 9:317–318.
- Noborio, K. 2001. Measurement of soil water content and electrical conductivity by time domain reflectometry: A review. *Comput. Electr. Agric.* 31:213–237.
- Oliver, B.M., and J.M. Cage. 1971. *Electronic measurements and instrumentation*. McGraw-Hill, New York.
- Or, D., J. VanShaar, R. Minnick, B. Fisher, R.A. Hubscher, and J.M. Wraith. 2003. WinTDR: A Windows-based time domain reflectometry program for measurement of soil water content and electrical conductivity. USU Soil Physics Group, Logan, Utah. Available at <http://soilphysics.usu.edu/wintdr> (verified 26 May 2004).
- Persson, M., and S. Haridy. 2003. Estimating water content from electrical conductivity measurements with short time-domain reflectometry probes. *Soil Sci. Soc. Am. J.* 67:478–482.
- Robinson, D.A., M. Schaap, S.B. Jones, S.P. Friedman, and C.M.K. Gardner. 2003a. Considerations for improving the accuracy of permittivity measurement using TDR: Air-water calibration, effects of cable length. *Soil Sci. Soc. Am. J.* 67:62–70.
- Robinson, D.A., S.B. Jones, J.M. Wraith, D. Or, and S.P. Friedman. 2003b. A review of advances in dielectric and electrical conductivity measurement in soils using time domain reflectometry. *Vadose Zone J.* 2:444–475.
- Topp, G.C., J.L. Davis, and A.P. Annan. 1980. Electromagnetic determination of soil water content: Measurements in coaxial transmission lines. *Water Resour. Res.* 16:574–582.
- Topp, G.C., S. Zegelin, and I. White. 2000. Impacts of the real and imaginary components of relative permittivity on time domain reflectometry measurements in soils. *Soil Sci. Soc. Am. J.* 64: 1244–1252.
- Ulaby, F.T., R.K. Moore, and A.K. Fung. 1986. *Microwave remote sensing: Active and passive from theory to application*. Vol. III. Artech House, Norwood, MA.
- van Gemert, M.J.C. 1973. High-frequency time-domain methods in dielectric spectroscopy. *Philips Res. Repts.* 28:530–572.
- Weerts, A.H., J.A. Huisman, and W. Bouten. 2001. Information content of time domain reflectometry waveforms. *Water Resour. Res.* 37:1291–1299.